Peeping in on the cytoskeleton: light microscopy approaches to actin and microtubule organization

Abhishek Sahasrabudhe, Vijay Vittal and Aurnab Ghose*

Indian Institute of Science Education and Research, 900 NCL Innovation Park, Dr Homi Bhaba Road, Pune 411 008, India

The actin and microtubule cytoskeletons consist of a dynamic network of polymer filaments that enable a variety of fundamental cellular processes, including cell shape, cell motility, chromosome separation and cytokinesis, synaptic plasticity, organelle distribution and intracellular transport and trafficking. Regional organization and remodelling of these filaments form the basis of their diverse critical functions and our ability to visualize these events with high spatio-temporal resolution is a powerful approach to uncover the cellular logic of cytoskeleton function. In recent years, a range of light microscopy techniques along with novel labelling and analytical tools has become available which allows unprecedented access to the cytoskeletal organization and dynamics. This article summarizes accessible technology platforms and strategies that allow one to peep into the inner life of these polymer systems.

Keywords: Actin, epifluorescence, light microscopy, microtubule, time-lapse imaging.

'You can observe a lot by watching.'

– Lawrence (Yogi) Berra

as quoted in *Sports Illustrated*, 1984, **60**(14), 94.

THE actin and microtubule (MT) cytoskeletons are critically involved in all aspects of cellular biology, including regulation of cell shape, cell polarization, cellular motility, chromosome segregation and cell division, intracellular trafficking and transport, muscle contraction, cell–cell interactions and synaptic plasticity[1–6]. These polymer systems are highly dynamic and are instructively remodelled by orchestrated biochemical interactions to achieve spatio-temporal specificity. The relative regional autonomy of polymer assembly/disassembly and supramolecular organization endows the cytoskeletal systems with structural specificity, which in the context of cell biology is translated to functional specificity[7,8]. The length and timescales these systems operate in are increasingly amenable to light microscopy approaches and this article summarizes some of the readily available epifluorescence imaging options that can be employed to study cytoskeleton organization and dynamics.

*For correspondence. (e-mail: aurnab@iiserpune.ac.in)

Cell biological tools to label actin and microtubules

Prior to microscopic evaluation, epifluorescence microscopy requires appropriate labelling of the structures under observation by fluorophore-tagged markers. For actin and MTs these include small molecules showing selective binding, peptide tags, immunodetection, expression of fluorophore-tagged actin/tubulin monomers to fluorophore-tagged actin/MT binding proteins as fiduciary labels.

The most common method of selectively labelling actin involves fluorescent derivatives of phallotoxins – bicyclic peptides isolated from *Amanita phalloides*[9]. These peptides selectively bind filamentous actin (F-actin) and not monomeric globular actin (G-actin) and appear to retain their affinity for F-actin across eukaryotic species (Figure 1). Deoxyribonulease (DNAse I) binds G-actin strongly and its fluorescent derivatives are commonly used to label this fraction of actin[10]. Both these agents require cell permeabilization and are therefore suitable largely for fixed samples.

Labelled purified actin is the reagent of choice in *in vitro* single-molecule reconstitution experiments studying polymer growth properties or filament displacement (for example, by associated motor proteins[11,12]). Live cell imaging studies have also used fluorophore-labelled purified actin, but these involve microinjection or other cumbersome protocols to deliver the reagent inside cells. Careful titration with endogenous monomers is necessary to avoid compromising actin functionality. On the other hand, this approach gives very tight control on the amount of labelled monomers that are introduced into the cell and is ideal for studies involving stochastic, sparse labelling strategies which can extract kinematic information (for example, fluorescence speckle microscopy discussed later). Expression of green fluorescent protein (GFP) or similar fluorophore-tagged actin is also used[13], though it is known that the fluorophore tag alters actin dynamics, especially when expressed in higher amounts[14]. Fusion of

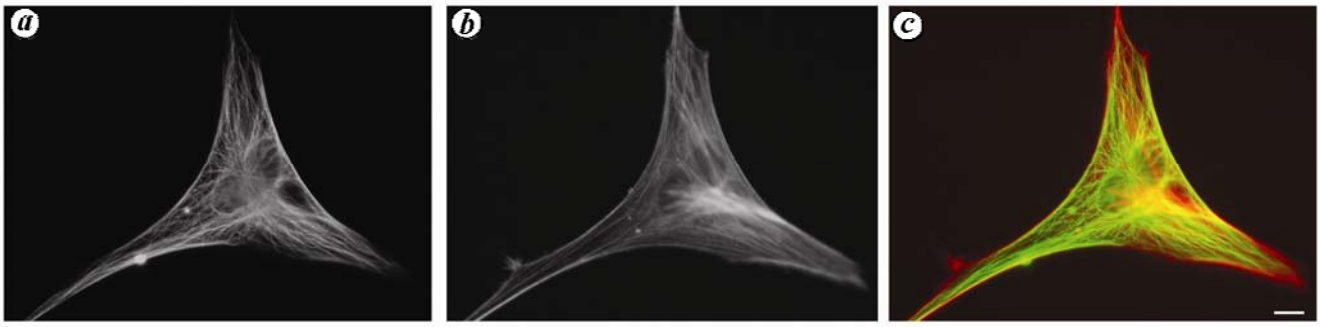

Figure 1. Widefield imaging of fixed NIH3T3 fibroblast. ***a***, Immunofluorescence using anti α-tubulin (Sigma). ***b***, F-actin labelled by fluorescent phalloidin (Molecular Probes®). ***c***, Merge (tubulin: green; actin: red). Scale bar = 5 μm.

actin-binding domains of proteins (like that of moesin) to GFP has also been successfully used[15]. However, these are typically large molecules and may compete with endogenous proteins and increase the probability of artifacts. Recently, a 17 amino acid peptide, named 'Lifeact', absent in all eukaryotes except yeast, has been isolated and its fluorophore-tagged derivatives have become the reagent of choice for labelling F-actin[16]. The relatively low affinity of Lifeact for actin reduces the chances of competition with endogenous actin-binding proteins and its absence in most eukaryotes eliminates the need for titrating against endogenous activities. Lifeact has been successfully used to visualize actin structures across phyla and to study actin dynamics in whole organisms, including fungi[17–19], nematodes, *Arabidopsis* and mice[20].

Immunofluorescence is a popular method for observing microtubule organization. Tubulin isoform-specific antibodies are commonly used (Figure 1) as are antibodies detecting tubulin-specific post-translational modifications like acetylation, tyrosination (Figure 2 *c*)[21]. The latter allow the evaluation of microtubule stability and its heterogeneity in space and time. These local differences in stability profoundly influence MT function[21,22].

As in the case of actin, labelled purified monomers of tubulin are used in *in vitro* reconstitution studies and have contributed greatly to our understanding of the behaviour of MT-associated motor proteins, kinesin and dynein[23,24]. These reagents have been extensively used in speckle microscopy, especially in the evaluation of MT dynamics in the mitotic asters.

Transfection of constructs expressing GFP (or equivalent) tagged tubulin is a widely used alternative for live cell imaging, though the issue of titrating against endogenous monomers remains a major concern[25–28]. In regions with a large number of MTs, this strategy is limited as the overlapping signals preclude the analysis of MT dynamics. However, GFP-tagged tubulin has been used to make transgenic flies, worms and fish, which show normal development and offer the opportunity to assess MT responses across development.

One of the most rewarding approaches to the study of MT dynamics has been the use of fluorophore-tagged MT plus tip interacting proteins (+TIPs). +TIPs are a group of proteins that localize to the growing plus ends of MTs[29]. Within this class, the end-binding protein (EB) family of proteins has been most extensively used[30] because of its relatively small size (~35 kDa) and ability to express it to detectable levels without affecting MT behaviour (Figure 3).

Fluorescent derivatives of paclitaxel (a di-terpenoid isolated from the plant *Taxus brevifolia*) bind polymerized beta tubulin[31]. Paclitaxel is cell permeable and consequently can be used in live imaging studies in low doses[32].

Common epifluorescence imaging modalities to visualize the cytoskeleton

Widefield fluorescence microscopy has been used successfully to image both the actin and MT cytoskeletons (Figure 1). In this mode, full-field illumination is used with all the emission light collected by the objective being sent to the detector. This remains a powerful imaging strategy, especially when combined with high-quantum efficiency, low-noise CCD cameras. The ability to combine widefield epifluorescence with transmitted light imaging modes like differential interference contrast (DIC) aids imaging by defining the spatial context of the structures under observation in the fluorescent mode. Typically, widefield imaging has been limited to flat samples, effectively two-dimensional, as out-of-focus signals increase image degradation in thicker samples.

For thicker samples with significant out-of-focus signals, laser scanning confocal microscopy (LSCM) is the favoured option to observe cytoskeleton organization. In this mode, a pinhole is used to eliminate the out-of-focus light leading to a marked improvement of the signal-to-noise ratio (SNR). Optical sections can thus be acquired in the *z*-axis with significantly improved clarity (Figure 2 *a–c*). Excellent three-dimensional reconstructions of the acquired optical sections are possible with current image rendering strategies and allow visualization of cytoskeleton architecture in the axial plane (Figure 2 *c* and *d*).

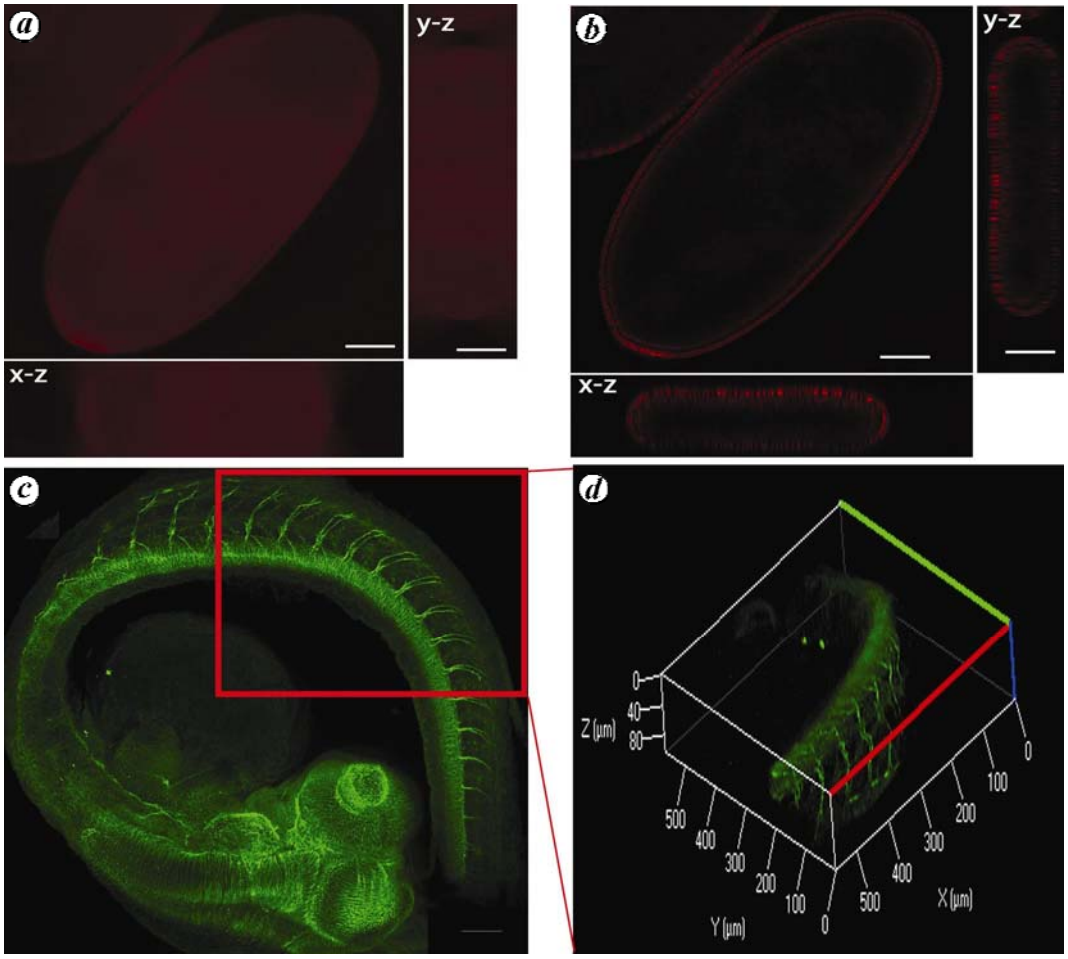

Figure 2. Comparison of widefield and point scanning LSCM in phalloidin-labelled early-stage *Drosophila* embryo. ***a***, Single optical section in widefield mode along with orthogonal projections in *y*–*z* and *x*–*z* planes. ***b***, Equivalent optical section using point scanning LSCM along with orthogonal projections. Scale bar = 50 μm. Note: There is significantly reduced out-of-focus information in the confocal optical section. Comparison of orthogonal views shows improved signal-to-noise ratio for the confocal image in the axial plane. ***c***, Whole-mount immunofluorescence using acetylated-tubulin antibody (Sigma) of a two-day-old zebrafish embryo labelling the developing nervous system. The image is a tiled maximum intensity projection of 75 optical sections covering a total depth of 104 μm. Scale bar = 50 μm. ***d***, Three-dimensional reconstruction of the marked region in (***c***).

Contrary to popular belief, confocal imaging of biological specimens typically does not improve lateral resolution sufficiently to access new information and the modest gain in axial resolution is achieved only with significant effort. On the other hand, the pinhole results in a ~20% loss of in-focus light, which may significantly reduce the useful signals reaching the detector[33]. Further, widefield microscopy with a cooled, low-noise camera introduces less noise in the image compared to LSCM[34]. The use of high-intensity lasers and the need to raster scan in LSCMs are often a hindrance to live cell applications because of increased photobleaching and relatively slower temporal resolution. In fact, widefield mode may be preferable over LSCM for specimens with low out-of-focus signals; particularly those being imaged live to access cytoskeleton dynamics.

Alternative confocal modes are available to increase the temporal resolution of LSCMs, which make use of multipoint scanning methods. Spinning disk confocal microscopy (SDCM) is one such solution that uses multiple pinholes to scan the sample simultaneously. It is well suited for live imaging applications as it efficiently removes out-of-focus light, while offering high acquisition rates[35]. The limitation of this method is the reduced axial resolution because of pinhole crosstalk, making it unsuitable for thick samples. Only a fraction of the laser intensity is transmitted through the spinning disk, making this technique incompatible with low-level fluorescence (increased exposure time negates the acquisition speed advantage). Both actin and MT behaviour has been studied quantitatively using SDCM in a range of biological specimens with high SNR[35].

Thick biological samples (> 100 μm) pose a problem for LSCM imaging. The full-volume LSCM illumination means that even though emission signals are collected only from the plane of focus, the fluorescence is generated

throughout the sample. In LSCM, the penetration depth is dependent on the scattering of the excitation and emission wavelengths by the specimen, and the absorption of the excitation energy along the entire beam path. This large excitation volume results in photobleaching and phototoxicity throughout the entire sample.

Two-photon excitation or two-photon confocal microscopy (TPCM) circumvents these issues by employing longer wavelength, lower energy excitation light to excite the fluorophore and therefore necessitates the simultaneous absorption of two photons to reach the requisite excitation energy[36]. The longer wavelengths scatter less in biological specimens and because of the multiphoton absorption requirement, the excitation volume is extremely small resulting in a strong suppression of background noise. Both these contribute to the greatly enhanced depth penetration achieved by TPCM. In addition, the longer red-shifted wavelengths are inherently less damaging to biological specimens than the more energetic shorter wavelengths. The other advantages of TPCM include the lack of pinholes and associated optics (as the probability of the two-photon absorption event is most likely only in the small focal point of the beam), resulting in minimal loss of emission signals. The geometry of the TPCM allows the detector to be placed close to the sample resulting in increased sensitivity. The advantages of TPCM have been employed successfully to study actin and MT organization in thick biological samples like brain tissue and whole-mount preparations of small organisms[37–40].

Blurring is a major source of image degradation caused by non-random diffraction of light as it passes through the lenses and the imaging system. Detailed models of blur are available in optical theory and can be applied to digital images to computationally remove blur[41]. Widefield microscopy collects both in-focus and out-of-focus light and allows blur to reach the detector. Deconvolution is a mathematical transformation applied to image data to remove blur or to reassign it to its source (Figure 4). With the development of better algorithms and computational power, widefield microscopy and deconvolution (WFD) have started to become popular. Broadly, there are two classes of these algorithms – 'deblurring' and 'image restoration'. The former operates typically by performing subtractive operations to each plane at a time in a 3D stack. The latter, in contrast, operates simultaneously on every pixel in a 3D stack reassigning it to its source. The subtractive nature of the 'deblurring' operations renders these images unsuitable for quantitative analysis, though significant qualitative improvement can be achieved. The constrained iterative versions of the 'image restoration'

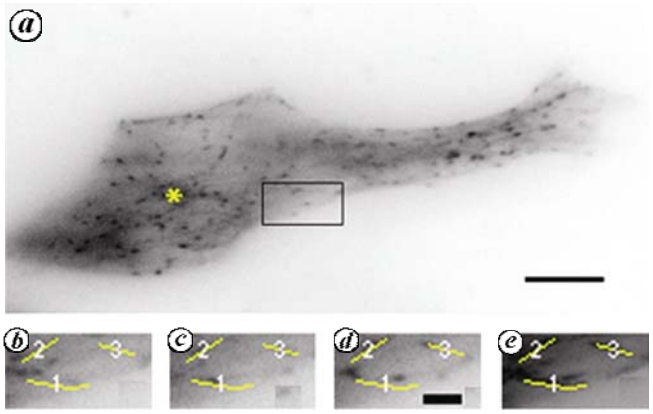

Figure 3. Microtubule dynamics in a NIH3T3 cell visualized using GFP-labelled EB3, a component of the microtubule +TIP complex. ***a***, Representative frame from a time-lapse series collected in TIRFM mode with an interval of 6 s between exposures. Asterisk marks the MT organizing centre. Scale bar = 10 µm. ***b–d***, Representative time-lapse frames from the boxed region used to demonstrate MT dynamics. The overlaid tracks in yellow represent the trajectories of three individual EB3 particles as determined from (***e***). ***e***, Collapsed time-series projection showing the EB3 trajectories used to analyse MT growth. Velocity analysis shows variable average speeds of 0.136 (particle-1), 0.1 (particle-2) and 0.16 µm/s (particle-3). Scale bar in (***d***) = 1 µm. Note: Images have been inverted for better visualization.

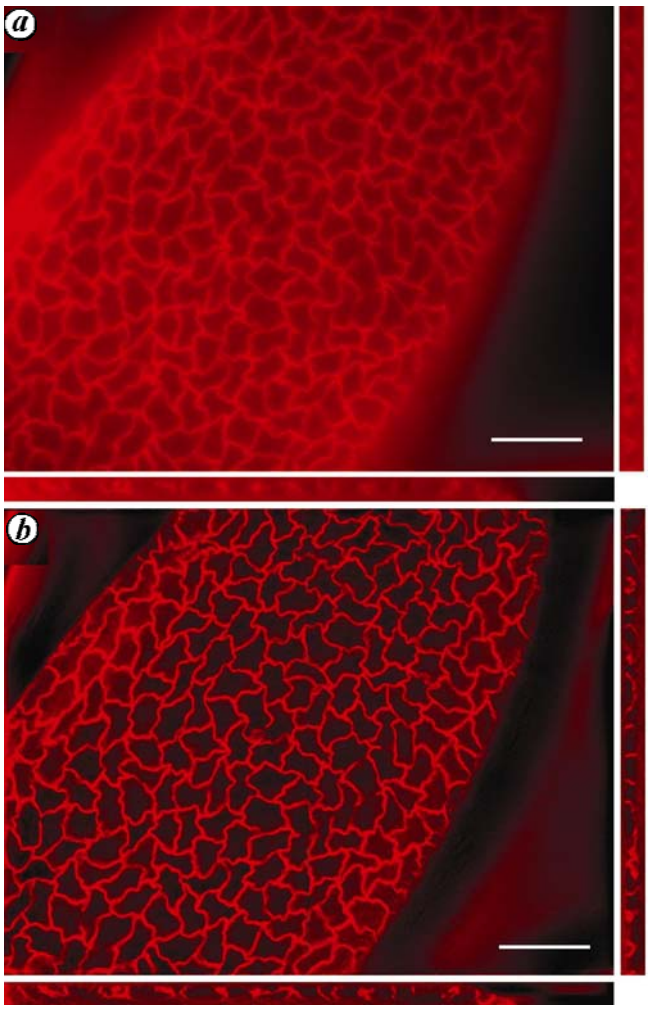

Figure 4. Comparison of widefield imaging and widefield acquisition followed by deconvolution. ***a***. Single optical section of phalloidin labelled early stage *Drosophila* embryo along with orthogonal projections. ***b***, Image of the same optical section following 3D deconvolution. Scale bar = 20 µm.

category can, if implemented carefully, retain the quantitative information. Various forms of WFD have been regularly used to observe the 3D architecture of the cytoskeleton in different tissues[34,42].

With the widespread use of LSCM, SDCM and WFD in recent years, their contrasting abilities have resulted in a need to establish empirical guidelines for choosing the most appropriate technology for live cell imaging. A direct, quantitative comparison of the three techniques has established that the ratio between the out-of-focus background and in-focus signal (haziness index, H) determines the extent of the useful range of these modalities[43]. For samples with low H (< 20), WHD is most appropriate, while SDCM is best for the intermediate range of H ($20 < H < 200$). For $200 < H < 1000$, the LSCM performs the best and for $H > 1000$ none of these modalities is useful.

Total internal reflection microscopy (TIRFM) is another fluorescence technique that allows the generation of high-contrast fluorescence images, with low background and almost negligible out-of-focus light[44]. This is achieved by total internal reflection of the excitation light at the coverglass–aqueous medium interface (where the sample is located) leading to the generation of an exponentially decaying evanescent wave of the same frequency. The exponential intensity decay of the evanescent wave limits the excitation of fluorescent molecules to a narrow excitation volume ranging from 50 to 200 nm from the surface of the coverglass. While this limits the applicability of TIRFM to cell surface phenomena, it leads to a huge increase in the SNR as there is virtually no out-of-focus signal or background (Figure 5). Because of these properties, TIRFM is the method of choice for single-molecule analysis, such as *in vitro* assays involving single actin or MT filament dynamics[45]. TIRFM is commonly used to improve SNR in live imaging studies involving accurate quantitation of MT and actin dynamics in live specimens[46–49]. We demonstrate this with an example in Figure 3, where time-lapse TIRFM is used to track the dynamics of MT growth. Cytoskeleton interaction with the cellular cortex, for example, cortical probing and capture of microtubules can be studied by TIRFM. Dynamics of cell-surface structures, like focal adhesions (macromolecular complexes coupling the cytoskeleton to the extracellular matrix) are also made accessible by TIRFM (Figure 5).

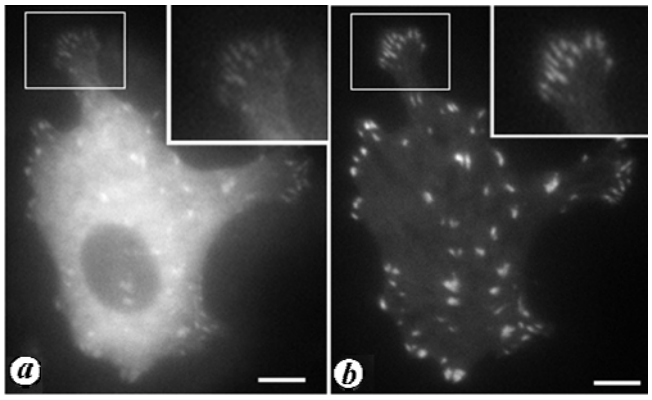

Figure 5. Comparison of widefield and TIRFM imaging of fluorophore-tagged vinculin, a focal adhesion marker, in NIH3T3 fibroblast. ***a***, Widefield image. ***b***, Same cell imaged in TIRFM mode showing improved signal-to-noise ratio. (Insets) Magnifications of the marked regions. Scale bar = 5 μm.

High-resolution fast imaging of large live samples

Selective plane illumination microscopy (SPIM) attempts to bring high-resolution, fast imaging to large, live samples (often whole organisms) typically imaged by low-resolution stereomicroscopy[50]. It uses a laser light-sheet to excite the entire focal plane simultaneously and selectively. By eliminating the temporally limiting beam scanning requirement as in CLSM, the acquisition rate is greatly enhanced. Further, the selective plane illumination strategy considerably reduces photobleaching and phototoxicity in the specimen, making it well suited for long-term imaging of live samples. In SPIM, the imaging axis is horizontal and the sample is positioned vertically allowing it to be turned for alignment or for imaging from different sides. The latter can be computationally merged to obtain improved isotropic resolution (same in lateral and axial planes) and enhanced uniformity in image quality, particularly in noisy samples[51].

Application of SPIM has led to the discovery of novel, intrinsic dynamics of MTs in *Xenopus*[18,52]. Studies using whole-mount nematode preparations have demonstrated the regulatory influence of the acto-myosin complexes on MT asters.

Going beyond Abbe's resolution limit

The diameters of individual F-actin (6 nm) or MT (25 nm) filaments are well below the resolution limit of standard light microscopes and there is a genuine need to study these structures at these length scales.

Resolution is defined as the shortest distance between two points on a specimen that can still be distinguished as two separate entities. An infinitely small point source of light imaged by a standard light microscope produces a blurred and diffracted, finite-sized focal spot at the image plane. The focal spot features progressively diminishing concentric rings (collectively known as the Airy disk) in the x–y plane and an elliptical 3D pattern along the z-axis called the point spread function (PSF)[53]. According to the Rayleigh two-point criterion, two adjacent points in the specimen are distributed by the imaging system as two PSFs and the width of these PSFs determine how close the two points can be and still be resolved by the microscope[53]. The size of the central spot in the Airy pattern

(x–y plane representation of the PSF) is related to the wavelength of light and the aperture angle of the objective (in essence the numerical aperture of the objective)[53]. Lateral resolution is thus defined by Abbe's formula as: resolution$_{x,y} = \lambda/2\text{NA}$, where λ is the wavelength of light and NA the numerical aperture of the objective. Therefore, using 400 nm light and a 1.4 NA objective, the resolution limit is ~150 nm in the x–y plane and approximately 450 nm axially.

Transgressions of Abbe's limit or the diffraction barrier have been attempted for almost a century, though the first breakthroughs came only in the 1990s, where 4Pi and I^{5}M techniques where developed that significantly improved axial resolution[54]. Improvements in far-field lateral resolution have come from two distinct strategies – PSF engineering and single-molecule localization microscopy. Multiple modalities based on these principles are now available and have contributed in making the actin–MT length scales accessible to light microscopy.

Stimulated emission depletion (STED) is a PSF engineering strategy that uses two synchronized laser pulses – one for excitation and the other to restrict the emission PSF by transferring the fluorophores to their ground state[55]. The depletion laser is engineered to have a zero-intensity node at the centre of focus so that fluorophores in this region are allowed to emit, while neighbouring fluorophores are depleted. The sequential readout of fluorescent probe photoswitching allows the constriction of the effective emission PSF (width is reduced), thereby increasing the resolution. STED microscopy with appropriate fluorophores can reach a lateral resolution of 30 nm.

Photoactivated localization microscopy (PALM) is a single-molecule technique based on the principle that a single-molecule can be spatially localized with extremely high accuracy if enough photons can be collected from it and if there is no interference from similarly emitting entities in close proximity (defined by Abbe's resolution limit). The approach involves repeated cycles of stochastic activation of fluorescence to intermittently turn on individual photoactivable molecules to a bright state, which are then imaged and photobleached. Thus signals from closely residing molecules (in the same diffraction-limited volume) are separated in time. Finally, merging of all single-molecule positions from the numerous iterations of activation and bleaching forms the final image. This technique is known to reach x–y resolutions of up to 20 nm.

The primary drawback of most readily available super-resolution methods is their relatively slow acquisition rates that limit their use in studying fast biological processes. In addition, some of the methodologies have complicated geometries, require additional lasers and sophisticated algorithms.

Both STED and PALM (and their sister techniques) have been used extensively to study actin and MT organization and the ability to access cytoskeleton filament-scale information has revealed hitherto unexpected observations[55]. For example, using stochastic optical reconstruction (STORM; a sister technique to PALM), an unanticipated periodic organization of actin in neuronal axons has been recently revealed[56].

Table 1 summarizes the relative strengths and weaknesses of the imaging modalities discussed above. Figure 6 offers a schematic representation of the resolution limits accessible by different imaging techniques.

Merging fluorescence and electron microscopy

Correlative light and electron microscopy (CLEM) involving transmitted light microscopy and electron microscopy (EM) has been employed in cytoskeleton research for some time[57]. However, merging fluorescence microscopy and EM is relatively new and has been gaining popularity in recent years as the limitations of labelling techniques, imaging hardware/software compatibilities and digital reconstruction have become significantly reduced. Fluorescence microscopy, as discussed above, allows for kinetic observations with high temporal resolution, while spatial resolution is limited. Conversely, high spatial resolutions are achievable by EM though it is limited to fixed samples. A detailed treatment of CLEM is beyond the scope of this article and it is included only to point out a new emerging dimension in imaging the cytoskeleton. Introduction of fluorescent probes, which are additionally capable of generating contrast for EM, has been a major impetus. These reagents include quantum dots, hybrid systems of synthetic fluorophores and targeting proteins, and genetically encoded fluorophores. For a comprehensive review, readers are referred to Giepmans[58].

Analytical techniques for studying cytoskeleton dynamics

The actin and MT cytoskeletons are highly dynamic entities, whose instructive remodelling underlies their diverse

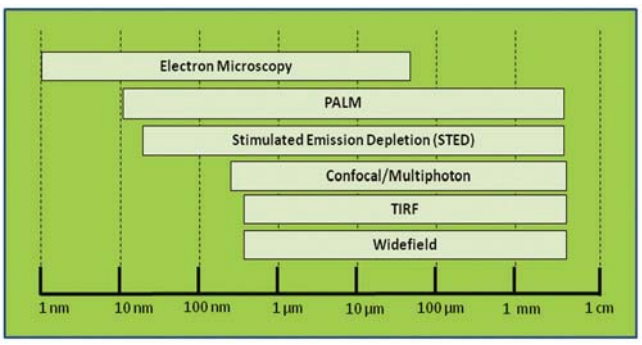

Figure 6. Schematic representation of lateral resolutions achievable by different fluorescent imaging modes.

Table 1. Summary of the relative advantages and disadvantages of various epifluorescence imaging techniques commonly employed in studying actin and microtubule organization. All abbreviations are introduced in the main text except STORM (stochastic optical reconstruction microscopy; a sister technique to PALM) and GSDM (ground-state depletion microscopy)

Microscopy technique	Advantages	Disadvantages
Widefield	Inexpensive compared to other techniques, works with a simple halide light source, wide range of available fluorophores.	Not useful for thick samples (out-of-focus blur), non-uniform spectrum of illumination, sample bleaching.
Confocal (point/line scanning)	Useful for thick samples, optical sectioning, more informative for co-localization studies, slight improvement on lateral resolution, specific excitation wavelength.	Expensive, requires lasers, slow, time-intensive, requires strong fluorophores, limited range of fluorophores, high-intensity lasers can be damaging to the tissue, sample bleaching.
Confocal (spinning disk)	Faster than point/line scanning, better for live samples.	Lower lateral resolution due to pinhole crosstalk.
Two-photon/multi-photon	Higher accessibility to deep tissue, low sample bleaching.	Expensive, additional fast-pulsed laser required, resolution is slighly compromised because of longer wavelengths used for excitation, limited range of fluorophores.
TIRF	High signal-to-noise ratio, improved *z*-resolution.	Limited to regions close to the coverglass.
Widefield deconvolution	Inexpensive, can be combined with conventional widefield imaging.	Can lead to artifacts if not used properly.
SPIM	Fast acquisition, high penetration depth, reduced sample bleaching and thus extended time-lapse imaging, isotropic resolution limits.	Unconventional set-up, expensive, not widely available in commercial market, may lead to artifacts during 3D rendering.
PALM (and STORM)	Highest possible resolution using optical imaging platforms.	Sophisticated algorithms, limited fluorophores, slow and thus not readily adapted for live/ dynamic samples.
STED (and GSDM)	Highest possible resolution using optical imaging platforms.	Requires additional lasers, slow, limited fluorophores, cannot be used for live samples.

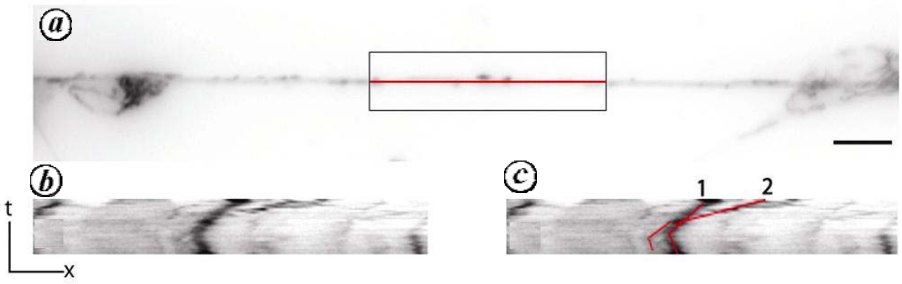

Figure 7. ***a***, Axonal mitochondria labelled with Mitotracker (Molecular Probes®). The cell body is towards the left and the growth cone towards the right. The red line within the boxed region in ***a*** has been selected to generate the kymograph, ***b***. ***c***, Same kymograph as ***b***, overlaid with red lines marking the dynamics of two mitochondria. For particle-1 direction of movement is initially retrograde with an average velocity of 0.004 μm/s before direction reversal. Particle-2 initially moves in the retrograde direction with an average velocity of 0.01 μm/s after which it slows down and reverses direction. Note: Images have been inverted for better visualization.

functions in cells. It is therefore essential to characterize the dynamics of these systems and develop analytical tools to extract dynamic information from time-lapse observations of cytoskeleton responses. Labelling strategies are critical for the extraction of kinetic information. For sparsely distributed signals with good SNRs, manual or semi-automated tracking can be used. Multiple tracking algorithms are available which typically treat the signal as a solid particle traversing through space and plot the trajectories of the centroid across time. This kind of analysis can provide detailed information on the directionality, extent and rate of displacement, instantaneous and average velocities, and dynamic organization in space. However, these tend to be limited to small regions of the cell and lower number of events being simultaneously analysed. Figure 3 *b–d* provides examples of tracking MT growth by following the signal from the +TIP protein, EB 3. Maximum intensity projections across the duration of the time-lapse can be made and the dynamical behaviour of the signal extracted from it.

Kymographs represent alternative to represent dynamic processes in a single image. These are *x–t* scans across a time-lapse series, where the intensity across a line is plotted for all images of the series (Figure 7). The direction of movement can be inferred from the trajectory of the signal in the kymograph, while the velocity can be determined from its slope.

Fluorescent speckle microscopy (FSM) is a method to study the dynamics of macromolecular complexes that have been extensively used to study movement and assembly/disassembly kinetics of actin and MT cytoskeletons[59]. This technique circumvents the twin problems of high background fluorescence and the inability to detect movement or subunit turnover in uniformly labelled fluorescent structures. FSM, unlike techniques involving photobleaching or photoactivation that give similar information, can deliver kinetic information across large areas of the cell with high spatio-temporal resolution. The stochastic incorporation of subunits from a mixed pool of labelled and unlabelled monomers into the macromolecular assembly (here the cytoskeleton filament) results in variations in the number of fluorescently labelled subunits in each diffraction-limited image region. This is the source of the speckled labelling pattern in FSM. Powerful image analysis and statistical treatments have been applied to the speckle patterns rendering it possible to use these as fiduciary markers of polymer assembly/disassembly kinetics, lifetime, velocity, movement and trajectory[59]. FSM has been tremendously successful in providing high-resolution, quantitative information on the dynamics of the actin and MT system in a number of biological scenarios. FSM combined with TIRFM has been recently used to demonstrate a hierarchical transmission of actin motion through the focal adhesions[47].

Conclusion

Quantitative microscopic analysis is an incisive tool to study the spatiotemporally diverse organization and function of actin and MT networks. Numerous imaging modalities are currently available, which when combined with appropriate labelling and analysis methods can be powerful tools to study cytoskeletal regulation. Selection of appropriate combinations of techniques vis-a-vis the specific cytoskeletal processes being probed is a critical step in successful experimental design. We hope this summary will point interested readers to the possibilities available and help them choose the most relevant approaches.

1. Carlsson, A. E., Actin dynamics: from nanoscale to microscale. *Annu. Rev. Biophys.*, 2010, **39**, 91–110.
2. Fletcher, D. A. and Mullins, R. D., Cell mechanics and the cytoskeleton. *Nature*, 2010, **463**, 485–492.
3. Gelfand, V. I. and Bershadsky, A. D., Microtubule dynamics: mechanism, regulation, and function. *Annu. Rev. Cell Biol.*, 1991, **7**, 93–116.
4. Hawkins, T., Mirigian, M., Selcuk Yasar, M. and Ross, J. L., Mechanics of microtubules. *J. Biomech.*, 2010, **43**, 23–30.
5. Lee, S. H. and Dominguez, R., Regulation of actin cytoskeleton dynamics in cells. *Mol. Cells*, 2010, **29**, 311–325.
6. Lowery, L. A. and Van Vactor, D., The trip of the tip: understanding the growth cone machinery. *Nature Rev. Mol. Cell Biol.*, 2009, **10**, 332–343.
7. Basu, R. and Chang, F., Shaping the actin cytoskeleton using microtubule tips. *Curr. Opin. Cell Biol.*, 2007, **19**, 88–94.
8. Huber, F. and Kas, J., Self-regulative organization of the cytoskeleton. *Cytoskeleton* (*Hoboken*), 2011, **68**, 259–265.
9. Vandekerckhove, J., Deboben, A., Nassal, M. and Wieland, T., The phalloidin binding site of F-actin. *EMBO J.*, 1985, **4**, 2815–2818.
10. Kabsch, W., Mannherz, H. G. and Suck, D., Three-dimensional structure of the complex of actin and DNase I at 4.5 A resolution. *EMBO J.*, 1985, **4**, 2113–2118.
11. Kron, S. J., Toyoshima, Y. Y., Uyeda, T. Q. and Spudich, J. A., Assays for actin sliding movement over myosin-coated surfaces. *Methods Enzymol.*, 1991, **196**, 399–416.
12. Waterman-Storer, C. M., Desai, A., Bulinski, J. C. and Salmon, E. D., Fluorescent speckle microscopy, a method to visualize the dynamics of protein assemblies in living cells. *Curr. Biol.*, 1998, **8**, 1227–1230.
13. Ballestrem, C., Wehrle-Haller, B. and Imhof, B. A., Actin dynamics in living mammalian cells. *J. Cell Sci.*, 1998, **111**(Pt 12), 1649–1658.
14. Westphal, M. *et al.*, Microfilament dynamics during cell movement and chemotaxis monitored using a GFP-actin fusion protein. *Curr. Biol.*, 1997, **7**, 176–183.
15. Edwards, K. A., Demsky, M., Montague, R. A., Weymouth, N. and Kiehart, D. P., GFP-moesin illuminates actin cytoskeleton dynamics in living tissue and demonstrates cell shape changes during morphogenesis in *Drosophila*. *Dev. Biol.*, 1997, **191**, 103–117.
16. Riedl, J. *et al.*, Lifeact: a versatile marker to visualize F-actin. *Nature Methods*, 2008, **5**, 605–607.
17. Berepiki, A., Lichius, A., Shoji, J. Y., Tilsner, J. and Read, N. D., F-actin dynamics in Neurospora crassa. *Eukaryot. Cell*, 2010, **9**, 547–557.
18. Redemann, S. *et al.*, Membrane invaginations reveal cortical sites that pull on mitotic spindles in one-cell *C. elegans* embryos. *PLoS One*, 2010, **5**, e12301.
19. Era, A. *et al.*, Application of Lifeact reveals F-actin dynamics in *Arabidopsis thaliana* and the liverwort, *Marchantia polymorpha*. *Plant Cell Physiol.*, 2009, **50**, 1041–1048.
20. Riedl, J. *et al.*, Lifeact mice for studying F-actin dynamics. *Nature Methods*, 2010, **7**, 168–169.
21. Janke, C. and Bulinski, J. C., Post-translational regulation of the microtubule cytoskeleton: mechanisms and functions. *Nature Rev. Mol. Cell Biol.*, 2011, **12**, 773–786.
22. Hammond, J. W., Cai, D. and Verhey, K. J., Tubulin modifications and their cellular functions. *Curr. Opin. Cell Biol.*, 2008, **20**, 71–76.
23. Niwa, S. *et al.*, KIF19A Is a microtubule-depolymerizing kinesin for ciliary length control. *Dev. Cell*, 2012, **23**, 1167–1175.
24. Waterman-Storer, C. M. and Salmon, E. D., Fluorescent speckle microscopy of microtubules: how low can you go? *FASEB J. Suppl. 2*, 1999, **13**, S225–S230.
25. Kimble, M., Kuzmiak, C., McGovern, K. N. and de Hostos, E. L., Microtubule organization and the effects of GFP-tubulin expression in *Dictyostelium discoideum*. *Cell Motil. Cytoskelet.*, 2000, **47**, 48–62.
26. Grieder, N. C., de Cuevas, M. and Spradling, A. C., The fusome organizes the microtubule network during oocyte differentiation in *Drosophila*. *Development*, 2000, **127**, 4253–4264.
27. Strome, S. *et al.*, Spindle dynamics and the role of gamma-tubulin in early *Caenorhabditis elegans* embryos. *Mol. Biol. Cell*, 2001, **12**, 1751–1764.

28. Asakawa, K. and Kawakami, K., A transgenic zebrafish for monitoring *in vivo* microtubule structures. *Dev. Dyn*., 2010, **239**, 2695–2699.
29. Gouveia, S. M. and Akhmanova, A., Cell and molecular biology of microtubule plus end tracking proteins: end binding proteins and their partners. *Int. Rev. Cell Mol. Biol*., 2010, **285**, 1–74.
30. Mimori-Kiyosue, Y., Shiina, N. and Tsukita, S., The dynamic behavior of the APC-binding protein EB1 on the distal ends of microtubules. *Curr. Biol*., 2000, **10**, 865–868.
31. Amos, L. A. and Lowe, J., How Taxol stabilises microtubule structure. *Chem. Biol*., 1999, **6**, R65–R69.
32. An, S., Deng, Y., Tomsho, J. W., Kyoung, M. and Benkovic, S. J., Microtubule-assisted mechanism for functional metabolic macromolecular complex formation. *Proc. Natl. Acad. Sci. USA*, 2010, **107**, 12872–12876.
33. Pawley, J. B., In *Handbook of Biological Confocal Microscopy*, Springer, 2006, pp. 20–41.
34. Swedlow, J. R., Hu, K., Andrews, P. D., Roos, D. S. and Murray, J. M., Measuring tubulin content in *Toxoplasma gondii*: a comparison of laser-scanning confocal and wide-field fluorescence microscopy. *Proc. Natl. Acad. Sci. USA*, 2002, **99**, 2014–2019.
35. Adams, M. C. *et al*., A high-speed multispectral spinning-disk confocal microscope system for fluorescent speckle microscopy of living cells. *Methods*, 2003, **29**, 29–41.
36. Benninger, R. K., Hao, M. and Piston, D. W., Multi-photon excitation imaging of dynamic processes in living cells and tissues. *Rev. Physiol. Biochem. Pharmacol*., 2008, **160**, 71–92.
37. Dombeck, D. A. *et al.*, Uniform polarity microtubule assemblies imaged in native brain tissue by second-harmonic generation microscopy. *Proc. Natl. Acad. Sci. USA*, 2003, **100**, 7081–7086.
38. Urban, N. T., Willig, K. I., Hell, S. W. and Nagerl, U. V., STED nanoscopy of actin dynamics in synapses deep inside living brain slices. *Biophys. J*., 2011, **101**, 1277–1284.
39. Vishwasrao, H. D., Trifilieff, P. and Kandel, E. R., *In vivo* imaging of the actin polymerization state with two-photon fluorescence anisotropy. *Biophys. J*., 2012, **102**, 1204–1214.
40. Wuhr, M., Obholzer, N. D., Megason, S. G., Detrich, H. W. and Mitchison, T. J., Live imaging of the cytoskeleton in early cleavage-stage zebrafish embryos. *Methods Cell Biol*., 2011, **101**, 1–18.
41. Biggs, D. S., 3D deconvolution microscopy. *Curr. Protocols Cytom*., 2010, Chapter 12, Unit 12.19, 1–20.
42. Littlefield, R. and Fowler, V. M., Measurement of thin filament lengths by distributed deconvolution analysis of fluorescence images. *Biophys. J*., 2002, **82**, 2548–2564.
43. Murray, J. M., Appleton, P. L., Swedlow, J. R. and Waters, J. C., Evaluating performance in three-dimensional fluorescence microscopy. *J. Microsci*., 2007, **228**, 390–405.
44. Millis, B. A., Evanescent-wave field imaging: an introduction to total internal reflection fluorescence microscopy. *Methods Mol. Biol*., 2012, **823**, 295–309.
45. Gell, C. *et al.*, Microtubule dynamics reconstituted *in vitro* and imaged by single-molecule fluorescence microscopy. *Methods Cell Biol*., 2010, **95**, 221–245.
46. Dixit, R. and Ross, J. L., Studying plus-end tracking at single molecule resolution using TIRF microscopy. *Methods Cell Biol*., 2010, **95**, 543–554.
47. Hu, K., Ji, L., Applegate, K. T., Danuser, G. and Waterman-Storer, C. M., Differential transmission of actin motion within focal adhesions. *Science*, 2007, **315**, 111–115.
48. Grigoriev, I. and Akhmanova, A., Microtubule dynamics at the cell cortex probed by TIRF microscopy. *Methods Cell Biol*., 2010, **97**, 91–109.
49. Berginski, M. E., Vitriol, E. A., Hahn, K. M. and Gomez, S. M., High-resolution quantification of focal adhesion spatiotemporal dynamics in living cells. *PLoS One*, 2011, **6**, e22025.
50. Huisken, J., Swoger, J., Del Bene, F., Wittbrodt, J. and Stelzer, E. H., Optical sectioning deep inside live embryos by selective plane illumination microscopy. *Science*, 2004, **305**, 1007–1009.
51. Huisken, J. and Stainier, D. Y., Selective plane illumination microscopy techniques in developmental biology. *Development*, 2009, **136**, 1963–1975.
52. Keller, P. J., Pampaloni, F. and Stelzer, E. H., Three-dimensional preparation and imaging reveal intrinsic microtubule properties. *Nature Methods*, 2007, **4**, 843–846.
53. Inoue, S. and Spring, K., *Video Microscopy*, Plenum Press, New York, 1986.
54. Bewersdorf, J., Schmidt, R. and Hell, S. W., Comparison of I5M and 4Pimicroscopy. *J. Microsci*., 2006, **222**, 105–117.
55. Willig, K. I., Rizzoli, S. O., Westphal, V., Jahn, R. and Hell, S. W., STED microscopy reveals that synaptotagmin remains clustered after synaptic vesicle exocytosis. *Nature*, 2006, **440**, 935–939.
56. Xu, K., Zhong, G. and Zhuang, X., Actin, spectrin, and associated proteins form a periodic cytoskeletal structure in axons. *Science*, 2012, **339**, 452–456.
57. Svitkina, T. M. and Borisy, G. G., Correlative light and electron microscopy of the cytoskeleton of cultured cells. *Methods Enzymol*., 1998, **298**, 570–592.
58. Giepmans, B. N., Bridging fluorescence microscopy and electron microscopy. *Histochem. Cell Biol*., 2008, **130**, 211–217.
59. Danuser, G. and Waterman-Storer, C. M., Quantitative fluorescent speckle microscopy of cytoskeleton dynamics. *Annu. Rev. Biophys. Biomol. Struct*., 2006, **35**, 361–387.

ACKNOWLEDGEMENTS. We thank Dr Richa Rikhy and Ms Aparna Sherlekar for preparing the samples used in Figures 2 *a*, *b* and 3. Mr Ratnakar Mishra helped prepare the sample used in Figure 2 *c* and *d*. We thank Prof. N. K. Subhedar for critically evaluating the early versions of this manuscript. A.S. is funded by a CSIR senior research fellowship and research in A.G.'s group is supported by extramural grants from the Department of Biotechnology and the Department of Science and Technology, Government of India. Intramural funding from IISER Pune is also acknowledged. All image acquisition and processing was done by us in IISER Pune's imaging facility.